PNAS RESEARCH ARTICLE | ENGINEERING

Actuation driven pseudocrease mechanics in multistable curved-crease origami shells

Kevin T. Liu[a], Tomohiro Tachi[b], and Glaucio H. Paulino[a,c,1]

Affiliations are included on p. 8.

Edited by John A. Rogers, Northwestern University, Evanston, IL; received October 28, 2025; accepted April 6, 2026

Shells are lightweight load-bearing structures found ubiquitously throughout nature and engineering. Reconfigurable structures can change form and function, while multistable ones enable fast, large shape changes and the ability to maintain a deformed shape without the continuous input of work. Here we present a general design method for multistable shells inspired by curved-crease origami and the differential geometry of developable surfaces. Through detailed analysis of a reference multistable shell, we show that the shell naturally concentrates deformation along a band which we term a "pseudocrease." We analyze the effect geometric parameters have on the mechanical behavior to provide an intuitive understanding of the mechanics underlying the multistability, in which bending and stretching energies within the shell compete. We validate the numerical models and trends through experiments using samples of varying geometries. The validation addresses applications across a variety of length scales and forms, including a magnetically controlled curved-crease robot capable of morphing, rolling, steering, and crawling. Our approach holds potential for designing reconfigurable shells with tailored stiffness, energy barrier, and shape across multiple application areas.

multistability | curved-crease origami | magnetic actuation | reconfigurable structures | soft robots

Shells, which are thin structures defined by a curved surface, provide an efficient way of supporting loads. They exist both in nature, as in eggshells, skulls, nutshells, leaves, and in engineering, as in machine parts, hydraulic structures, aircraft, and bridges (1). Since ancient times, thin shells have been used as light-weight and form efficient structural elements due to their ability to transmit load through stretching and bending effects (2). Applications can be found in mechanical, aerospace, marine, and civil engineering fields.

Simultaneously, reconfigurable structures which are able to change their form and function have uses across engineering fields. Examples range from commonplace objects such as deployable umbrellas to advanced deployable space structures. Each configuration of a reconfigurable structure has its own advantages, such as compactness, rigidity, or a desired shape, and the ability to transition between configurations allows a single structure to exploit multiple advantages.

Some reconfigurable structures are multistable, in which energy barriers separate each configuration, which are local minima of potential energy. Multistable structures have the added advantage of maintaining a static position and resisting loads without requiring continuous energy input or additional locking mechanisms. In addition, they can rapidly achieve large shape-changing by releasing stored potential energy. For instance, in nature, one can find the Venus flytrap, which snaps together in a fraction of a second to capture insects (3).

Therefore, by combining the ability of shells to efficiently carry load with the ability to transform, a general design method that can create reconfigurable, multistable shells is attractive for potential engineering applications that require deployability, rapid shape change, or design flexibility. In the literature, bistable shells have been achieved through carefully designed layups in composites (4) and through prestress (5–7). However, these are limited to relatively simple geometries and accomplished through intricate material processing, rather than geometrically. Other multistable sheets consist of multiple bistable units such as invertible domes (8, 9) or curved-crease units (10), which can interact to generate a global deformation. Similarly, Meeusen et. al. (11) showed that introducing interacting defects to corrugated sheets can also create global deformation. In contrast, our work investigates multistable shells where the entire surface deforms together.

Significance

Reconfigurable, multistable shells are efficient, load-bearing structures which have applications ranging from architecture to aerospace and soft-robotics. We introduce a design framework for creating multistable shells inspired by curved-crease origami. Existing multistable shells are often limited in their achievable geometries, and frequently derive their multistability from specific material properties and/or prestress. In contrast, we present a purely geometric framework, which is applicable to any developable surface and can be combined with multiple curved creases to form complex multistable structures. The method is applicable to multiple length scales involving both contact and noncontact methods. This work opens avenues for creating reconfigurable structures with tailored properties across multiple engineering disciplines.

Author contributions: K.T.L., T.T., and G.H.P. designed research; K.T.L. and T.T. performed research; K.T.L. and G.H.P. contributed new reagents/analytic tools; K.T.L. analyzed data; and K.T.L. and G.H.P. wrote the paper.

The authors declare no competing interest.

This article is a PNAS Direct Submission.

[1]To whom correspondence may be addressed. Email: gpaulino@princeton.edu.

This article contains supporting information online at https://www.pnas.org/lookup/suppl/doi:10.1073/pnas.2530458123/-/DCSupplemental.

Published June 15, 2026.

A potential source of inspiration comes from curved-crease origami. Origami is an ancient art of paper folding, and in recent times has become the geometric inspiration for engineering applications across multiple length scales (12). There are multiple examples of multistable origami-inspired structures (13–15). Typically, the multistability comes from either an incompatibility in the energy stored in the fold creases or an incompatibility in the panel geometries that prevent rigid panel folding (12).

Although conventional origami patterns use straight creases, patterns with curved creases are also possible. However, unlike conventional origami, wherein the only deformation occurs at the crease lines, curved-crease origami also involves bending of the panels (16). Curved origami was first used as an artistic form due to its ability to make elegant yet complex shapes. Recently, with the introduction of mathematical frameworks to describe curved origami, practical engineering applications have been developed (17–21).

The literature on curved-crease origami can be roughly grouped based on what energies are considered. Early works analyzed the shape of curved-crease origami through the lens of developable surface theory, without any energy considerations (22–24). In this way, they explore what developable surfaces are geometrically feasible without considering which shapes are energetically favorable. Other works consider the impact of shell bending energy in geometries where shell stretching energy can be neglected (10, 21, 25, 26). Last, a smaller subset of works explicitly considers bending and stretching energy (19, 27, 28).

Curved origami with multistability has also been explored (10, 17–19, 27–29). Bende et al. provided a general mechanistic explanation of the existence of bistability in creased surfaces with a given natural curvature, focusing on three surfaces with positive (sphere), zero (cylinder), and negative (helicoid) Gaussian curvature (27). However, most examples of multistable curved origami that have been studied are limited to variations of a single geometry or are limited in their ability to be combined to form more complex multistable structures (18, 19, 29).

In this work, we present a design method for creating multistable shells inspired by curved-crease origami. We consider the mechanics of a curved surface involving energy due to bending and stretching, and consider the entire transition between stable states. We employ geometric arguments to qualitatively explain the mechanics in service of practical engineering designs. The nonlinearity of the deformation precludes using purely analytical methods, so numerical methods are used to simulate the deformation and complement the geometric analysis.

The paper is organized as follows. To motivate the present work, we begin by presenting a modern application of multistable shells with curved-crease origami robots actuated via noncontact methods. Such multistable structures are described using the theory of developable surfaces. In order to gain an intuitive understanding of their underlying mechanics, we examine a reference geometry (cylindrical shell with planar creases) in detail. We describe the behavior of associated physical models, then replicate that behavior using finite element analysis. In doing so, we find the potential for additional stable states to exist, which are not predicted by the theory, and we explain the reason for their existence. Next, we vary the geometric parameters and examine the effect on the stable states and energy barriers. We perform experimental validation for a variety of geometries and confirm the ability for the numerical models to accurately predict the mechanical behavior and trends of the physical models. We provide examples of generalizations of the method applied to cylindrical and conical surfaces, and nonplanar creases. Last, we provide applications ranging from bistable structures that could be used as electrical switches on the centimeter scale, a bistable box on the 10s of centimeters scale, and a multistable bench on the meter scale to show the scalability and broad applicability of the method.

Results

Magnetically Actuated Robot. As a demonstration of the design method, we fabricated a curved-crease robot which can morph, crawl, steer, and roll using noncontact actuation, as shown in Fig. 1 and Movie S1. Magneto-mechanical actuation is achieved when an external magnetic field is applied to a permanent magnet. A permanent magnet can be approximated as a magnetic dipole with magnetization $\mathbf{m}$, which in the presence of an external magnetic field $\mathbf{B}$, generates a magnetic torque $\mathbf{T} = \mathbf{m} \times \mathbf{B}$. Through controlling the external magnetic field, mobile robots can be controlled without contact (30), with designs based on different origami patterns seen in the literature (31–33).

As shown in Fig. 1, the curved-crease robot has two identical permanent magnets with opposite magnetization directions in the initial state. As a result, the curved-crease robot has no net magnetization. A perpendicular magnetic field generates opposing torques on each magnet, and a sufficient field magnitude can actuate the robot to the second stable state, which is enabled by the multistability of our design method. Now, each magnet has rotated, giving the robot a net magnetic field. In this actuated state, the robot can be steered or rolled using rotating fields, as shown in the bottom central figure.

Additionally, applying a magnetic field with an $\hat{\mathbf{x}}$ component will generate a torque which will act to increase the normal force on one foot and decrease the normal force on the other. As a result, during actuation the friction will be biased toward one foot, allowing the opposite foot to slide freely. By cyclically varying the magnetic field direction, bidirectional crawling can be achieved, as shown in the bottom left figure.

Last, we demonstrated our method's ability to design robots with different energy barriers. In the bottom right figure, the white, yellow, and red robots have increasing energy barrier. Therefore, by exerting a torque sufficient to actuate only the white robot, we can selectively actuate the white robot while the yellow and red robots remain unchanged. Then, the white robot can be rolled, while the yellow and red do not move because they have zero net magnetization in the original state. The magnetic curved-crease robot demonstrations are shown in Movie S1.

Theoretical and Mathematical Basis for Multistability. To explain the mathematical basis for multistability, we turn to developable surface theory. For a shell with thickness of t, the extensional stiffness scales with the thickness t, while the bending stiffness scales with the cube of the shell thickness t^3 (2). In the limit of a thin shell with vanishing thickness, the resistance to bending becomes negligible compared to that of stretching, which causes the shells to behave effectively inextensibly. Under this assumption, any surface achieved by bending an initially flat sheet is developable, having zero Gaussian curvature at all points. As all developable surfaces are ruled surfaces, potential folded shapes can be described by sets of rule lines which follow mathematical constraints (22).

Suppose that we are given a fixed space curve $\mathbf{X}(u)$ as a directrix and a flat patch with a defined boundary curve $\mathbf{x}(u)$. We are asked to solve for the shape that results from bending the flat patch such that the boundary curve matches the directrix.

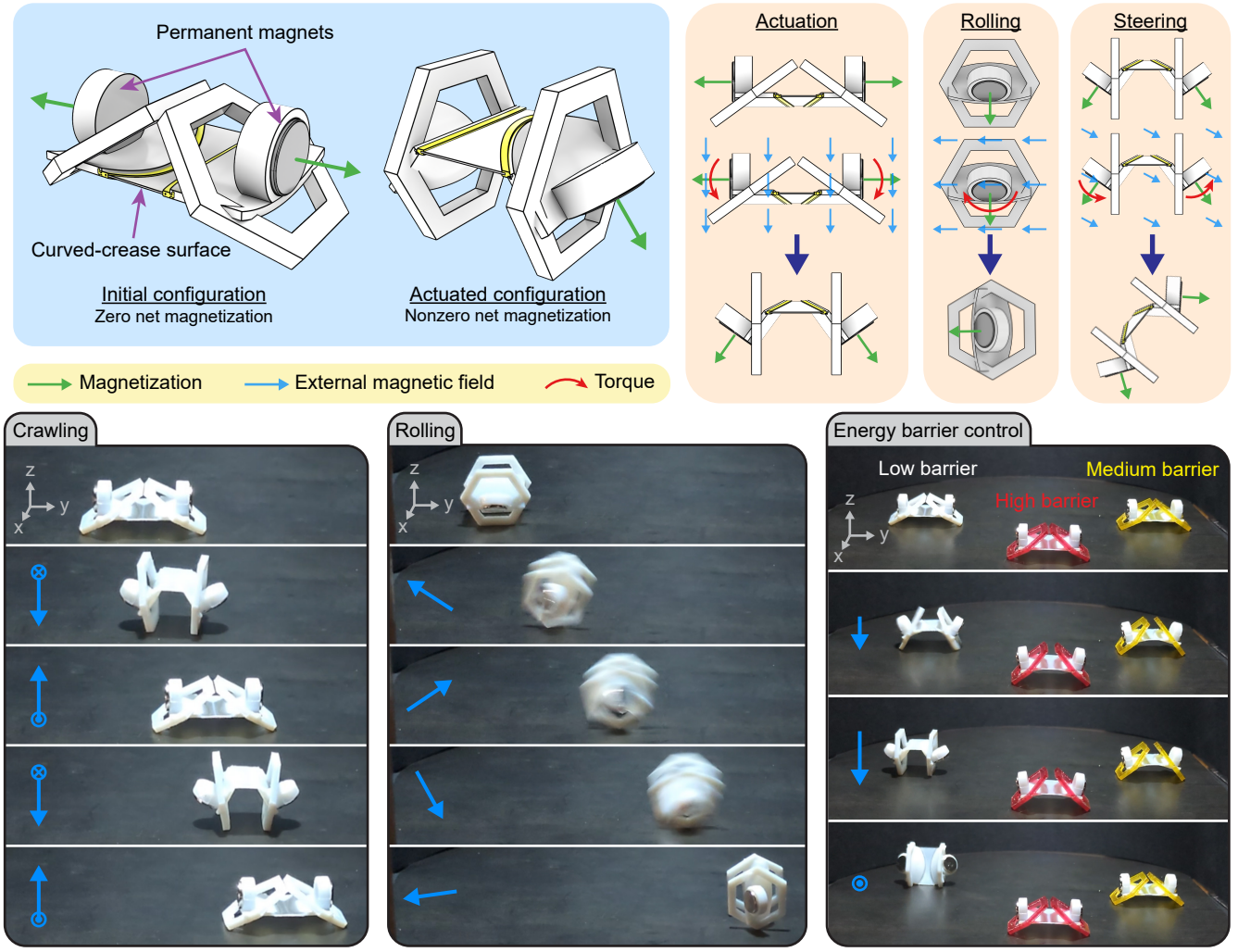

Fig. 1. Magnetically actuated curved-crease robot. The design of the robot is shown in the *Top Left*, with a central, bistable curved-crease surface and two identical permanent magnets. In the initial configuration, the magnetization directions are opposing, resulting in zero net magnetization. When actuated, the magnetization directions align, resulting in a net magnetization. In the *Top Right*, actuation, rolling, and steering modes under external magnetic fields are represented. In the *Bottom* we show snapshots of crawling, rolling, and energy barrier control demonstrations shown in Movie S1, with directions of the applied magnetic field depicted on the *Left*. Crawling is achieved by applying an actuating field while simultaneously applying a field in the $\hat{\mathbf{x}}$ direction, which creates a friction anisotropy between the two feet of the robot.

A ruled surface with directrix $\mathbf{X}(u)$ can be defined by a one-parameter family of lines by

$$\mathbf{S}(u, v) = \mathbf{X}(u) + v\mathbf{R}(u), \qquad [1]$$

for $u \in U = [0, u_{\max}]$ and $v \in \mathbb{R}$. The unit direction vectors $\mathbf{R}(u) : U \to S^2$ are the ruling directions at different points on the directrix. The ruled surface can also be described with five scalar functions $K(u)$, $\tau(u)$, $s(u)$, $\varphi(u)$, and $\theta(u)$. The first three functions are the curvature, torsion, and arc-length of the directrix, which are used classically through the Frenet–Serret formulas to describe curves in three-dimensional space (34). The inclination angle $\varphi(u)$ is the signed angle between the osculating plane of the directrix and the tangent plane of the surface. The ruling angle $\theta(u)$ is the angle between the rule line and the tangent direction of the directrix (23).

Applying the developability condition

$$K(u)\sin\varphi(u)\cot\theta(u) = -\tau(u) + \frac{\varphi'(u)}{s'(u)} \qquad [2]$$

and solving the Frenet–Serret formulas, it can be shown (23) that if the magnitude of the directrix curvature $K(u)$ exceeds that of the planar boundary curve $k(u)$, there exists exactly two different isometric or stretch-free configurations that the flat patch can be bent into, which satisfy

$$\varphi(u) = \pm\arccos\frac{k(u)}{K(u)}. \qquad [3]$$

The two solutions correspond to the positive or negative value of φ. Note that $k(u)$ is also the geodesic curvature of the directrix, because geodesic curvature is an intrinsic quantity. See the geometric analysis in *SI Appendix*, section 1 for more details.

A consequence of this result from differential geometry is that any configuration other than the two previously found will require surface stretching, creating a significant energy barrier between two low energy stretch-free states.

Next, to translate this result to curved-crease origami, suppose a crease divides a curved surface into patches P and Q. If the shape of patch P is made rigid, the crease also becomes rigid, creating the boundary conditions necessary for multistability. Patch Q has exactly two isometric configurations which satisfy Eq. **3**, which can become the stable states in a multistable structure.

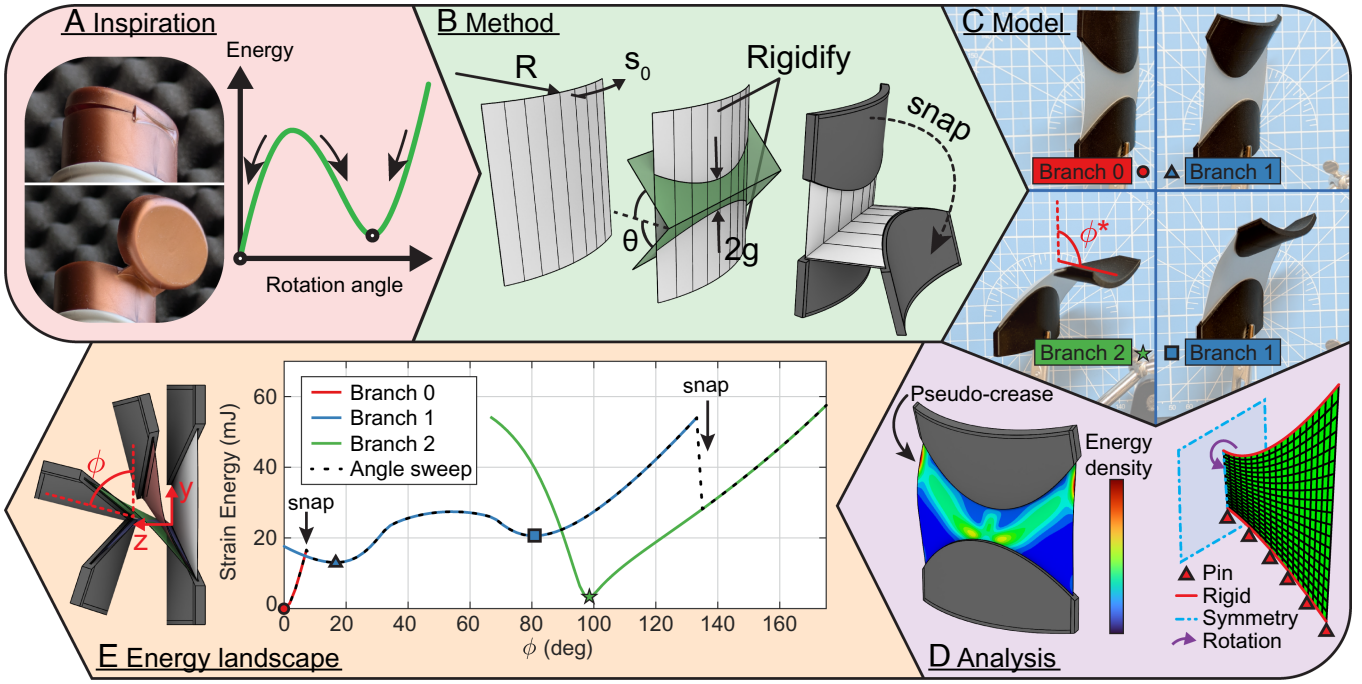

Fig. 2. (*A*) Plastic cap featuring a "butterfly" hinge design with conceptual bistable strain energy diagram. (*B*) Diagram showing design method to create bistable shells. For a given developable surface, creases are defined and portions of the surface are rigidified. A cylindrical model with two planar creases is shown with radius of curvature R, semiarc length s_0, crease plane inclination angle θ, and gap between creases $2g$. (*C*) Physical models showing the predicted stable states and additional intermediate stable states. The fold angle of the top handle ϕ^* at the second stable state is indicated. (*D*) Finite element boundary conditions and simulation result colored by strain energy density. The strain energy density is concentrated in a band we term a "pseudocrease." (*E*) Strain energy plot derived from numerical simulations, showing distinct deformation branches and the path along and between the branches as the top handle is rotated. The stable states seen in the model in (*C*) were successfully replicated in the simulation.

This theoretical result provides an explanation for the bistable behavior seen commonly in plastic cap hinges such as the one shown in Fig. 2*A*, in which a compliant shell is constrained along its edges along a curved crease. From the theoretical result, we propose a method for creating multistable structures, which is illustrated in Fig. 2*B*. We begin with any developable surface. We define a curved crease by the intersection of the surface and a plane. Last, we rigidify the shape of the surface on one side of the crease, creating the multistable structure. Based on this method, we produced the multistable prototypes shown in Fig. 2*C*, analyzed their mechanics using finite element methods shown in Fig. 2*D*, resulting in the energy landscapes shown in Fig. 2*E*, which confirm the multistable result seen in the inspiration for the work, the plastic bottle cap hinge design seen in Fig. 2*A*.

Here we assumed planar creases for simplicity. In this special case, the two isometric configurations of the free surface correspond to the initial surface and its reflection about the crease plane (35). This guarantees that boundary curves maintain the same shape between isometric configurations, allowing multiple rigid constraints surrounding a given compliant surface, as in Fig. 2*B*. Applying additional geometric constraints in this way increases the energy barrier between isometric states; however, the bistable result only requires one rigid constraint. Examples of geometries constraining only one crease and nonplanar creases are discussed in *Generalizations and Applications* and in *SI Appendix*.

Transitions between Stable States. While the geometric modeling predicts two stretch-free states for each curved-crease, it does not predict the nature of the transition between these stretch-free states. As an illustrative example, we examined in detail a reference multistable sample designed using the proposed method. We intersected two planes inclined at angles $\pm\theta$ from the horizontal with a cylindrical extrusion of a circular arc with radius of curvature R and semiarc length s_0, as shown in Fig. 2*B*. Next, we rigidified the top and bottom surfaces.

A physical sample was constructed using $R = 55$ mm, $\theta = 65°$, $s_0 = 30$ mm, and $g = 6$ mm out of a 0.5 mm thick polypropylene sheet. We found that the sample snaps to the predicted reflected shape, as shown in Fig. 2*C*. However, we also found additional unexpected intermediate stable states (Movie S2).

To understand the deformation and existence of intermediate states, we conducted numerical simulations, with boundary conditions and loads illustrated in Fig. 2*D*. The compliant central panel was modeled with shell elements. The bottom edge was pinned to the ground, and the top edge was pinned to a rigid body. A rotation was applied quasi-statically to the top surface, and the deformed shape and strain energy were recorded. Detailed descriptions of the numerical model are described in *SI Appendix*, section 2. A snapshot of the deformed shape colored by strain energy density is shown in Fig. 2*D*.

Deformation traces. To display the motion path of the structure, we traced the position and orientation of the top rigid body. Because of the symmetry assumption, the position can be expressed by two coordinates, which we chose to be the y and z coordinates of the central point, and the orientation can be expressed by a rotation angle ϕ. We found that not all branches of deformation found in the physical samples are accessible through applied rotation alone. Therefore, in a separate simulation, point forces were applied to the top handle at select times to transition the structure to a new branch (*SI Appendix*, section 2).

The trace of the motion path from two simulations are combined in Fig. 3 *A* and *B*. In Fig. 3*A*, we see that the tracked

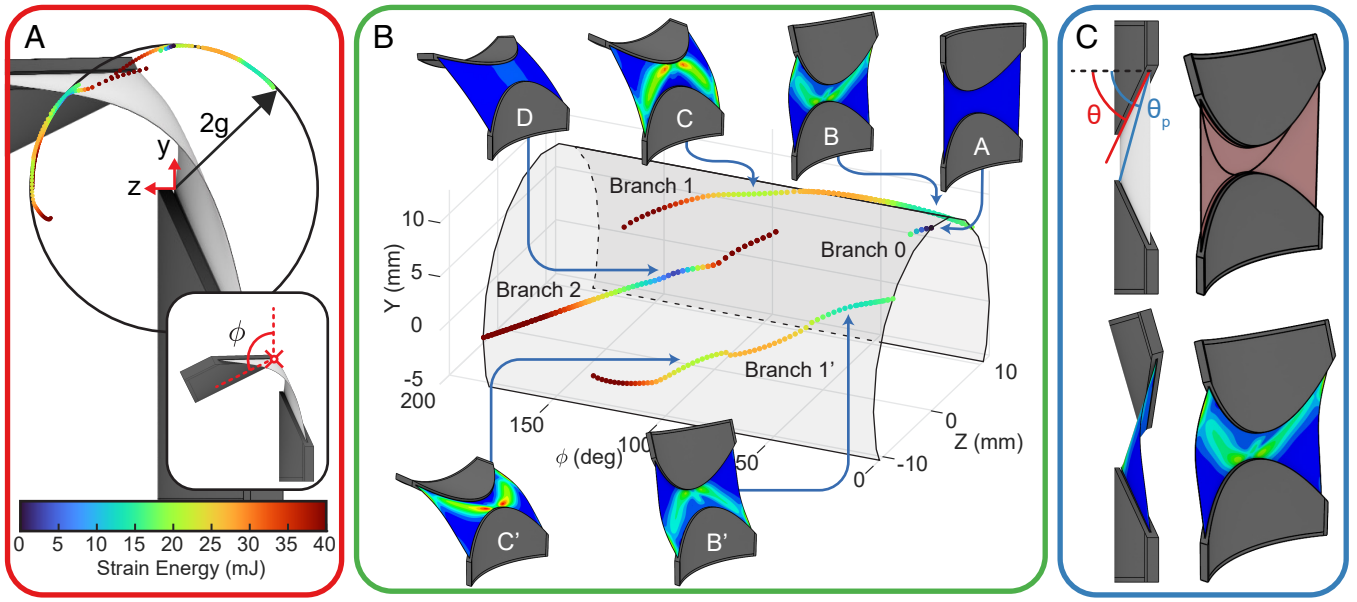

Fig. 3. (*A*) Diagram tracing the position of the point on the top handle highlighted red in the *Inset*. Each point is colored by the total strain energy in the system. The displacement paths generally trace a circle centered at the origin with radius 2*g*, with deviations resulting in high strain energy. (*B*) Plot of the points in (*A*) in *y* and *z* directions with the addition of the rotation angle ϕ of the top handle in a three-dimensional plot. One can observe distinct deformation branches. The deformed shapes of local minima of strain energy are depicted, with elements colored by strain energy density. (*C*) Comparison between the predicted and simulated geometry for stable state *B*. The *Top Left* figure indicates the predicted reflection planes at the top crease and a pseudocrease lying in a plane inclined at angle $-\theta_p$, and the *Top Right* figure shows the predicted shape in red assuming a sharp pseudocrease. The figures on the *Bottom* are two different views of the simulated shape colored by strain energy density. The modeled sample has parameters ($R = 55$ mm, $s_0 = 30$ mm, $\theta = 65°$, $g = 6$ mm, $t = 0.5$ mm).

point generally traces a circle centered at the origin with a radius equal to the gap between the two handles. At times, the tracked point moves away from the circle, which corresponds to high levels of strain energy, likely because a high degree of bending and stretching is required.

In Fig. 3*B*, we plotted the same data in a three-dimensional plot with the handle rotation angle ϕ plotted in the third axis. We can observe that the structure follows distinct branches through the state space. As the applied handle angle is varied, the structure follows along a stable branch. If the branch becomes unstable for a given handle angle, the structure will snap to a nearby stable branch. Along each branch, the total strain energy varies. The branches can be thought of as local minimum energy paths through the state space, and these paths determine the shape and size of the energy barrier between stable states. Fig. 2*E* plots the strain energy as a function of rotation angle ϕ for each branch found, and the black dotted line traces the path the sample follows as it jumps from branch to branch as the top handle angle is monotonically increased.

Stable states and pseudocreases. States of locally minimum energy are highlighted in Fig. 3*B*. We can observe that the intermediate stable states observed in the physical model are replicated in the simulation. Observing the energy density in these intermediate states shows that the energy is concentrated along a band which roughly lies in a plane containing the ends of one crease and the center of the opposite crease. This can be interpreted as the generation of a pseudocrease, where bending is localized along a thin band, rather than a diffuse deformation, similar to localization shown in indented shells (36) and traveling folds in curved origami bounded by a Sarrus linkage (28). A close correspondence between the simulated intermediate shape and geometric modeling assuming a sharp pseudocrease supports this argument, which is shown in Fig. 3*C* and is described in more detail in *SI Appendix*, section 3. The predicted pseudocrease planes have an inclination angle which minimizes the fold angle along the pseudocrease and reduces the bending energy.

For the given geometry, we found four distinct branches achievable from rotation. Qualitatively, Branch 0 has no creases folded with some central wrinkles, Branch 1 and 1′ have one crease folded and one pseudocrease, and Branch 2 has both creases folded. Branches 1 and 1′ are mirror reflections of each other. Different geometries can have additional branches, as shown in *SI Appendix*, section 4.

In *SI Appendix*, section 5, we decompose the strain energy into its stretching (U_S) and bending (U_B) components. We find that for small rotations, the stretching energy dominates, consistent with beam bending theory. When the first snap occurs, the stretching energy decreases while the bending energy increases, with total energy decreasing. We find that as the shell thickness is varied, the stretching and bending energies do not scale as $\propto t$ and $\propto t^3$, respectively, as expected, as the equilibrium geometry varies in order to minimize the total strain energy. For instance, if the thickness increases, the radius of curvature for a pseudocrease also increases, relieving some bending energy while increasing the stretching energy, analogous to results found in the crumpling of thin elastic sheets (37). As a result, the simulations show the bending energy increases slower than the expected $\propto t^3$ rate, stretching energy increases faster than the expected $\propto t$ rate, and total strain energy increasing slower than the rate expected by scaling the U_S and U_B by t and t^3, respectively, and summing.

In *SI Appendix*, section 6, we varied the geometric parameters of the curved-crease samples and observed the effect on the mechanical behavior. We found that by controlling variables such as the plane angle θ, radius of curvature R, arc-length s_0, and shell thickness t, we can design multistable shells with desired stiffness, peak load, number of stable states, and rotation angle.

Experimental Validation. To validate the accuracy of the numerical models, we conducted loading experiments. We constructed the samples by first 3D printing rigid handles from PLA plastic

and laser cutting the crease pattern out of a flat polypropylene sheet. The polypropylene sheets were then inserted into the PLA handles. Note that because the polypropylene sheets were initially flat, they were prestressed, causing a tendency for the sheets to flatten as the distance increases from the rigid handles, as shown in *SI Appendix*, section 9. This results in a decreased moment of inertia and a lower energy barrier than for a cylindrical geometry.

Fig. 4*A* shows the experimental setup using a displacement-controlled universal testing machine. Lever arms were attached to the base of each handle, which were secured to a rotational bearing fixture attached to the tester. This allows the lever arms to freely rotate, resulting in the tester applying only a vertical force to the lever arm. The curved-crease sample then experiences a vertical force in addition to a bending moment that is a function of the horizontal distance. More detailed diagrams and CAD images are shown in *SI Appendix*, Fig. S11. When the tester head descends, the sample rotates and snaps. For each sample, we repeated the experiment three times. The average load is plotted in Fig. 4*B* along with an uncertainty interval. However, because the results are very repeatable, the uncertainty intervals are only visible near the snaps.

From the experiments, we observe an initial high stiffness, a peak load, then a snap as one of the creases folds. The samples continue to fold and the load continues to increase. Depending on the geometric parameters, the sample may snap a second time at the second crease. Then, in the reverse direction, hysteresis can be observed due to dissipation and different branches that the sample follows.

We replicated this setup in numerical models. The simulated results are shown in the bottom half of Fig. 4*B*. We find good correspondence visually between the deformation sequence. Additional experimental results from different geometries are shown in *SI Appendix*, Fig. S11.

The simulations and experiments have good agreement, confirming the trends predicted by simulations. However, there are some differences between simulations and experiments. The experiments show a significant drop in the load at each snap, while the simulations tend to have a more gradual decrease in load. Additionally, the initial stiffness of the simulations tends to be greater than that of the sample. For simplicity, various details were not modeled in the simulations which can explain differences with the experiments. The simulations do not model the crease stiffness, while the samples are precreased, in which the material at the crease is plastically deformed, which acts to make the snap more dramatic. Rather than elastic, the polypropylene sheet is a viscoelastic material, which causes a rate dependence on the load profile. In addition, from 3D scans of the physical samples (*SI Appendix*, section 14), the physical samples tend to "flatten" more than the simulations predict, which could explains the lower initial stiffness than that predicted in the simulated elastic model.

Generalizations and Applications. Generalizing from the baseline sample geometry previously analyzed, our method is applicable to a wide variety of developable surfaces. Fig. 5*A* shows the method applied to an extrusion of periodically joined circular arcs, resulting in a long, snapping hinge. In addition, the method is not restricted to cylindrical surfaces, as Fig. 5*B* and *SI Appendix*, Fig. S15 show the result of applying the method to periodically joined conical surfaces.

Fig. 5*C* shows a shell which can be reconfigured to multiple shapes. We also show that we are able to design multistable structures that snap to a desired shape, such as the heart shape shown in Fig. 5*D* and the letters "PU" in Movie S5.

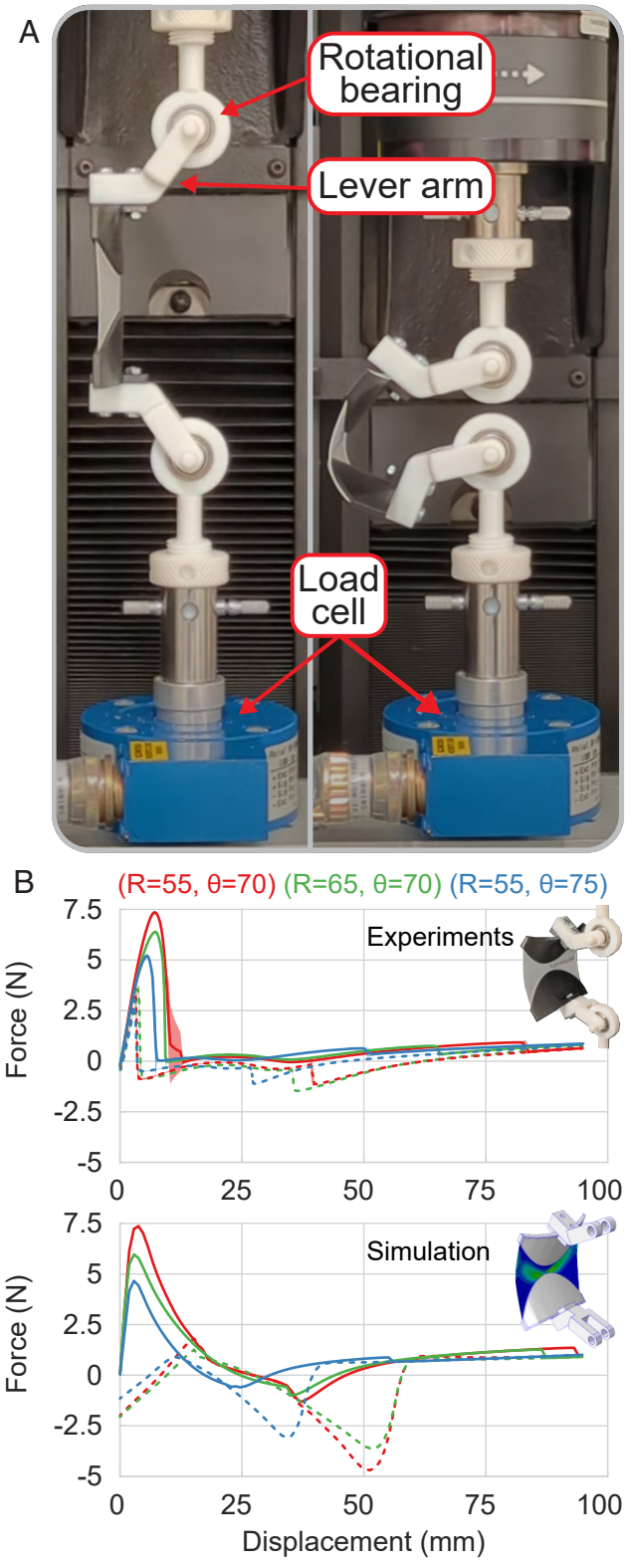

Fig. 4. (*A*) Experimental setup (*B*) Load vs. displacement plots for 3 samples with different geometric parameters (R, θ). $(s_0 = 30, g = 6, t = 0.5)$ for each sample. Length measurements are given in mm and angle measurements are given in degrees. For each sample, the average load is plotted with an uncertainty interval. However, because the results are very repeatable, the uncertainty intervals are only visible near the snaps. The solid lines represent the loading portion, while the dotted lines represent the unloading portion, when the tester head moves upward. From the tests shown, one can observe that increasing the radius of curvature decreases the peak load and increasing the inclination angle θ decreases the peak and shifts the second stable state leftward. Additional experiments and simulations varying all geometric parameters are shown in *SI Appendix*, section 9.

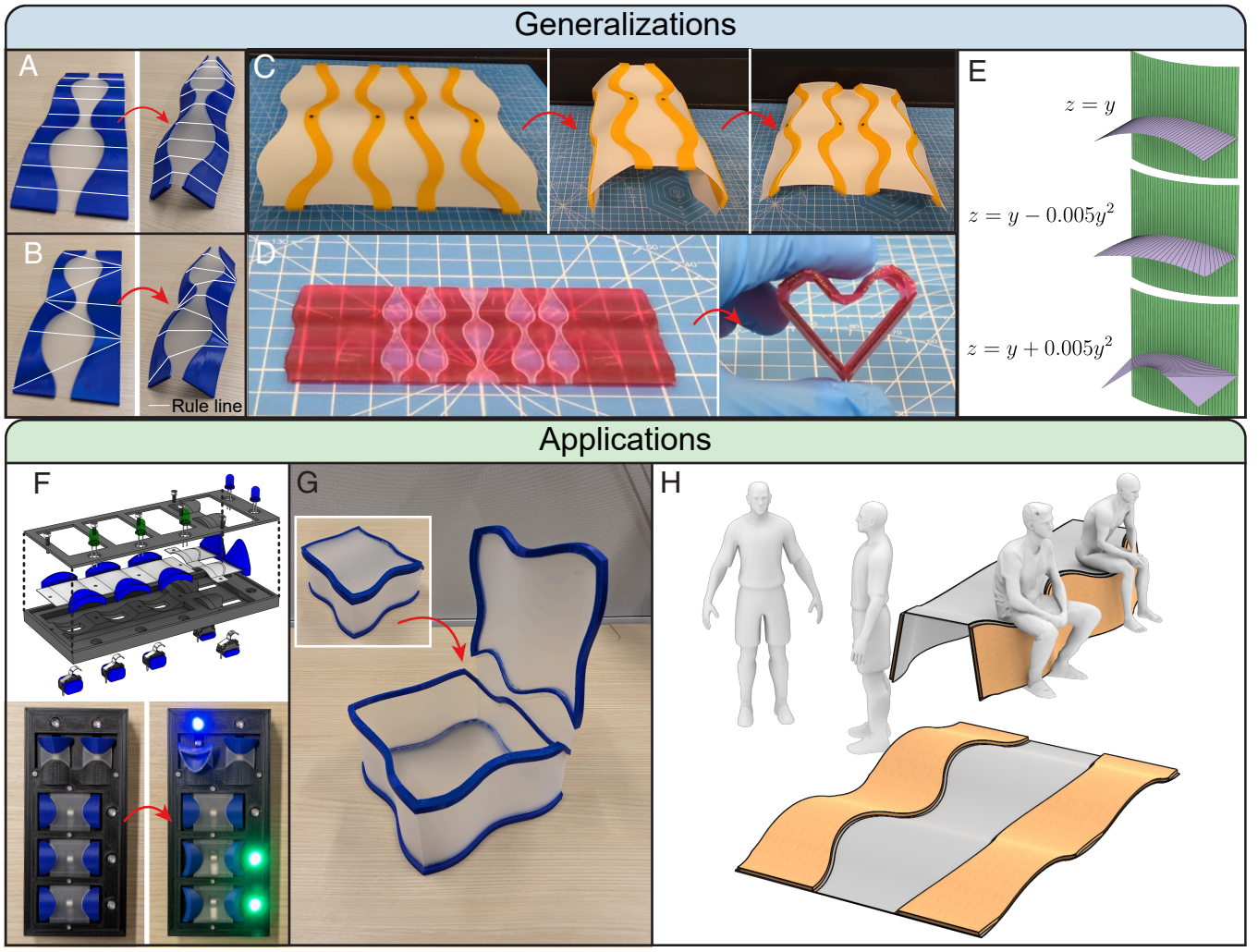

Fig. 5. Generalizations and applications. Multistable long hinges formed from a cylindrical (*A*) extrusion and conical (*B*) surfaces with rule lines. (*C*) Reconfigurable sheet. (*D*) Multistable strip which is designed to fold into a heart shape. (*E*) CAD images of stable states resultant from planar and nonplanar creases. (*F*) CAD diagram and physical model of snapping electrical switches. (*G*) Box with snapping hinge. (*H*) CAD image of a reconfigurable bench.

The multistable result can also be applied to nonplanar creases, provided that the two isometric configurations are physically possible (no intersecting rule lines, surface discontinuities, and surface self-intersections). Adding small adjustments to make a crease nonplanar can result in large differences in the isometric surface shapes shown in Fig. 5*E*. The mathematical modeling of the isometric states, numerical simulations, and physical prototypes are discussed in *SI Appendix*, section 11.

The method is suitable for a variety of application areas at a range of length scales. The method can be used to design intricate yet simple mechanisms, such as the electrical switches shown in Fig. 5*F*, which use multistability to maintain on/off status. We show two different switch designs. The two switches at the top are flip-switches, which resemble toggle light switches. The bottom three switches are turned on by pushing the central shell, which causes the blue handles to snap upward. To turn the switch off, the outer blue handles are pushed down and outward. Notably, the switch requires both hands to turn off, resembling two-handed safety switches, which are used to ensure operators' hands are kept out of harm's way.

Next, the method could be used in consumer products and packaging to create hinges that snap open and closed, such as the box shown in Fig. 5*G*. The method provides a versatile way to create hinges with tailored rest angles and stiffnesses.

At an architectural scale, the method could be used to design reconfigurable shelters or furniture which can be shipped in a compact, nearly flat configuration before being reconfigured into a shape that can sustain load, such as the foldable bench shown in Fig. 5*H*.

The snapping of the physical models in Fig. 5 as well as additional models are shown in Movie S5.

The proposed method provides designers a high degree of freedom for stable state geometry and load profile, while remaining elegant and only requiring a small number of parts. Because of the generality of the design method, there are potential applications in various fields and length scales beyond what has already been shown. For example, applications in soft robotics may take advantage of strain energy storage and high speed snapping for jumping or swimming applications. Such multistable shells have also potential applications in energy harvesting, energy damping, sequential folding for transport or deployment, and more.

Discussion

Inspired by curved-crease origami and the differential geometry of developable surfaces, we introduced a design method to create multistable shells starting from any developable surface.

The method entails defining curved creases and rigidifying portions of the shell, resulting in a finite number of stretch-free configurations which are separated by energy barriers.

To analyze the mechanics governing the transition between stretch-free states, we conducted numerical simulations. We found the existence of intermediate stable states with pseudocreases, which are validated in physical models. We analyzed the decomposition of strain energy into its stretching and bending components, and found a complex scaling with shell thickness. Additionally we simulated the impact of varying geometric parameters on mechanical properties, and found that the choice of parameters affects initial stiffness, energy barrier, existence of intermediate states, and the angle of folding for the stable states.

To validate the numerical models, we designed test fixtures, conducted experiments with a universal testing machine, and found good agreement with the numerical results. We found that the trends predicted in simulations were validated in experiments.

We then applied the design method to various more general geometries, including long, snapping hinges made from cylindrical and conical surfaces, and shells with nonplanar creases. We showed shells that can be reconfigured into multiple shapes, or designed to match a desired shape. Last we showed some example application areas in which the method could be utilized. Our design method is general to many geometries, able to be used repeatedly to make complex multistable shapes, and applicable on multiple scales. The method holds promising potential for designing reconfigurable shells with tailored stiffness, energy barrier, and shape.

Materials and Methods

Geometry Generation. Crease patterns and handle geometry files were generated using Rhino and Grasshopper modeling software. STL files were automatically generated using Grasshopper to create rigid fixtures that the flexible sheet could be inserted into.

Sample Fabrication. The shell surfaces were laser-cut from 0.4 mm and 0.5 mm polypropylene film using a Universal Laser PLS6.150D laser cutter. The crease lines were cut partially through the thickness of the film on the "mountain" side of the crease. Handle fixtures which fix the curvature of portions of the shell were manufactured out of PLA using a UltiMaker S3 printer. The polypropylene shell was then inserted into the handles. Last, the samples were manually folded in order to prefold the creases.

Instron Test Fixture. The Instron test fixture shown in Fig. 5*A* were printed using a Stratasys J55 3D printer using Vero resin and assembled with a rotational bearing. The load test was conducted with an Instron 68SC-5 Universal Testing System.

UV-Printed Samples. The curved-crease robot, heart sample shown in Fig. 5*E*, and the PU in Movie S5 were printed using a Stratasys J55 3D printer using Vero resin for the shell surface and elastico, a soft flexible elastomer, for creases.

Data, Materials, and Software Availability. Python and Grasshopper scripts are openly available at Zenodo (38). All other data are included in the article and/or supporting information.

ACKNOWLEDGMENTS. We acknowledge Princeton-UTokyo Strategic Partnership, "Princeton Catalysis Initiative" (PCI) at Princeton University, NSF Award No. 2323276, JST JPMJKB2302, and JSPS KAKENHI 24H00822 for funding support. Any opinions, findings and conclusions or recommendations expressed in this material are those of the authors and do not necessarily reflect the views of the sponsors. We thank Konstantinos Manos for his guidance in circuit design for the electrical switch model, and Dr. Xiangxin Dang for useful discussions.

Author affiliations: [a]Department of Civil and Environmental Engineering, Princeton University, Princeton, NJ 08544; [b]Department of General Systems Studies, Graduate School of Arts and Sciences, The University of Tokyo, Tokyo 153-8902, Japan; and [c]Princeton Materials Institute, Princeton University, Princeton, NJ 08544

1. E. Ventsel, T. Krauthammer, E. Carrera, Thin plates and shells: Theory, analysis, and applications. *Appl. Mech. Rev.* **55**, B72–B73 (2002).
2. C. R. Calladine, *Theory of Shell Structures* (Cambridge University Press, 1983).
3. Y. Forterre, J. M. Skotheim, J. Dumais, L. Mahadevan, How the venus flytrap snaps. *Nature* **433**, 421–425 (2005).
4. S. Guest, S. Pellegrino, Analytical models for bistable cylindrical shells. *Proc. R. Soc. A: Math. Phys. Eng. Sci.* **462**, 839–854 (2006).
5. E. Kebadze, S. Guest, S. Pellegrino, Bistable prestressed shell structures. *Int. J. Solids Struct.* **41**, 2801–2820 (2004).
6. A. Norman, K. Seffen, S. Guest, Multistable corrugated shells. *Proc. R. Soc. A: Math. Phys. Eng. Sci.* **464**, 1653–1672 (2008).
7. K. A. Seffen, S. D. Guest, Prestressed morphing bistable and neutrally stable shells. *J. Appl. Mech.* **78**, 011002 (2011).
8. J. P. Udani, A. F. Arrieta, Programmable mechanical metastructures from locally bistable domes. *Extreme Mech. Lett.* **42**, 101081 (2021).
9. M. Liu, L. Domino, I. D. de Dinechin, M. Taffetani, D. Vella, Snap-induced morphing: From a single bistable shell to the origin of shape bifurcation in interacting shells. *J. Mech. Phys. Solids* **170**, 105116 (2023).
10. M. Mirzajanzadeh, D. Pasini, Reprogrammable curved-straight origami: Multimorphability and volumetric tunability. *Sci. Adv.* **11**, eadu4678 (2025).
11. A. Meeussen, M. Van Hecke, Multistable sheets with rewritable patterns for switchable shape-morphing. *Nature* **621**, 516–520 (2023).
12. D. Misseroni *et al.*, Origami engineering. *Nat. Rev. Methods Primers* **4**, 40 (2024).
13. B. Kresling *et al.*, "Natural twist buckling in shells: From the hawkmoth's bellows to the deployable Kresling-pattern and cylindrical Miura-ori" in *Proceedings of the 6th International Conference on Computation of Shell and Spatial Structures* (International Association for Shell and Spatial Structures, Ithaca, NY, 2008), vol. 11, pp. 12–32.
14. K. Liu, P. P. Pratapa, D. Misseroni, T. Tachi, G. H. Paulino, Triclinic metamaterials by tristable origami with reprogrammable frustration. *Adv. Mater.* **34**, 2107998 (2022).
15. J. L. Silverberg *et al.*, Using origami design principles to fold reprogrammable mechanical metamaterials. *Science* **345**, 647–650 (2014).
16. S. J. Callens, A. A. Zadpoor, From flat sheets to curved geometries: Origami and kirigami approaches. *Mater. Today* **21**, 241–264 (2018).
17. T. U. Lee *et al.*, Self-locking and stiffening deployable tubular structures. *Proc. Natl. Acad. Sci. U.S.A.* **121**, e2409062121 (2024).
18. M. Lee, M. Abu-Saleem, T. Tachi, J. Gattas, "A lightweight building construction system using curved-crease origami blocks" in *8th International Meeting on Origami in Science, Mathematics and Education* (2024).
19. Y. Jiang *et al.*, Ultra-tunable bistable structures for universal robotic applications. *Cell Rep. Phys. Sci.* **4**, 101365 (2023).
20. H. Y. Patil, K. J. Maki, E. T. Filipov, Rapidly deployable hulls and on-demand tunable hydrodynamics with shape morphing curved crease origami. *J. Fluids Struct.* **130**, 104176 (2024).
21. Z. Zhai, Y. Wang, K. Lin, L. Wu, H. Jiang, In situ stiffness manipulation using elegant curved origami. *Sci. Adv.* **6**, eabe2000 (2020).
22. D. A. Huffman, Curvature and creases: A primer on paper. *IEEE Trans. Comput.* **100**, 1010–1019 (1976).
23. D. Fuchs, S. Tabachnikov, More on paperfolding. *Am. Math. Mon.* **106**, 27–35 (1999).
24. C. Jiang, K. Mundilova, F. Rist, J. Wallner, H. Pottmann, Curve-pleated structures. *ACM Trans. Graph. (TOG)* **38**, 1–13 (2019).
25. T. U. Lee, Z. You, J. M. Gattas, Elastica surface generation of curved-crease origami. *Int. J. Solids Struct.* **136**, 13–27 (2018).
26. M. A. Dias, L. H. Dudte, L. Mahadevan, C. D. Santangelo, Geometric mechanics of curved crease origami. *Phys. Rev. Lett.* **109**, 114301 (2012).
27. N. P. Bende *et al.*, Geometrically controlled snapping transitions in shells with curved creases. *Proc. Natl. Acad. Sci. U.S.A.* **112**, 11175–11180 (2015).
28. S. Chai, Z. Hu, Y. Chen, Z. You, J. Ma, Programmable multi-stability of curved-crease origami structures with travelling folds. *J. Mech. Phys. Solids* **193**, 105877 (2024).
29. J. Flores, L. Stein-Montalvo, S. Adriaenssens, Effect of crease curvature on the bistability of the origami waterbomb base. *Extrem. Mech. Lett.* **57**, 101909 (2022).
30. Y. Kim, X. Zhao, Magnetic soft materials and robots. *Chem. Rev.* **122**, 5317–5364 (2022).
31. Q. Ze *et al.*, Soft robotic origami crawler. *Sci. Adv.* **8**, eabm7834 (2022).
32. S. Miyashita, S. Guitron, M. Ludersdorfer, C. R. Sung, D. Rus, "An untethered miniature origami robot that self-folds, walks, swims, and degrades" in *2015 IEEE International Conference on Robotics and Automation (ICRA)* (IEEE, 2015), pp. 1490–1496.
33. G. Chung, J. W. Chae, D. S. Han, S. M. Won, Y. Park, Reprogrammable, recyclable origami robots controlled by magnetic fields. *Adv. Intell. Syst.* **6**, 2400082 (2024).
34. M. P. Do Carmo, *Differential Geometry of Curves and Surfaces: Revised and Updated* (Courier Dover Publications, ed. 2, 2016).
35. J. Mitani, Column-shaped origami design based on mirror reflections. *J. Geom. Graph.* **16**, 185–194 (2012).
36. A. Vaziri, L. Mahadevan, Localized and extended deformations of elastic shells. *Proc. Natl. Acad. Sci. U.S.A.* **105**, 7913–7918 (2008).
37. A. Lobkovsky, S. Gentges, H. Li, D. Morse, T. A. Witten, Scaling properties of stretching ridges in a crumpled elastic sheet. *Science* **270**, 1482–1485 (1995).
38. K. T. Liu *et al.*, Actuation driven pseudo-crease mechanics in multistable curved-crease origami shells. Zenodo. https://doi.org/10.5281/zenodo.16883914. Deposited 26 January 2026.